IEEE Access
Multidisciplinary | Rapid Review | Open Access Journal

Received September 4, 2020, accepted September 18, 2020, date of publication September 30, 2020,
date of current version October 21, 2020.

Digital Object Identifier 10.1109/ACCESS.2020.3027825

Multi-Modal Data Fusion Using Deep Neural Network for Condition Monitoring of High Voltage Insulator

**DAMIRA MUSSINA, (Associate Member, IEEE),
AIDANA IRMANOVA, (Associate Member, IEEE),
PRASHANT K. JAMWAL, (Senior Member, IEEE),
AND MEHDI BAGHERI, (Senior Member, IEEE)**
Electrical and Computer Engineering Department, Nazarbayev University, 010000 Astana, Kazakhstan

Corresponding author: Damira Mussina (damira.pernebayeva@nu.edu.kz)

This work was supported by the Faculty Development Competitive Research Grants, Nazarbayev University, under Grant 090118FD5322.

ABSTRACT A novel Fusion Convolutional Network (FCN) is proposed in this research for potential real-time monitoring of insulators using unmanned aerial vehicle (UAV) edge devices. Precise airborne imaging of outdoor objects, such as high voltage insulators, suffers from varied object resolution, cluttered backgrounds, unclear or contaminated surfaces, and illumination conditions. Accurate information about the insulator surface condition is essential and is of a high priority since insulator breakdown is a leading cause of electrical failure. A multi-modal information fusion (MMIF) system is developed during this research to analyze and classify possible contaminations present on the electrical insulators. A novel system, referred to as FCN, consists of a Convolutional Neural Network (CNN) and a binary Multilayer Neural Network (MNN) sub-classifier. While constructing the MMIF dataset for training and testing the novel FCN, the image classification output of the CNN is combined with the leakage current values (LCV) obtained as the classification output of MNN. Each sample of the MMIF dataset is, therefore, represented as a series of fusions. Later, sub-classifiers, of the FCN, are trained to identify the contamination types in the fusion series by implementing a voting system of sub-classifiers which is trained to identify a given class. As a result of the implementation of the proposed FCN, the classification accuracy increased by 8.4%, i.e., from 92% to 99.76%. To compare and benchmark the performance of proposed FCN, conventional classification algorithms are also implemented on the fusion of features that are extracted employing the wavelet transform and PCA methods. State-of-the-art CNN architectures are also discussed on account of their time consumption and memory usage. The conceptualization of a potential hardware implementation of the proposed FCN, on emerging edge devices, is also provided for completeness of the discussion. Pertinent outcomes of this research can be further extended to other potential applications of airborne imaging.

INDEX TERMS Convolutional neural network, multi-modal information fusion, electrical insulators, unmanned aerial vehicle.

I. INTRODUCTION

Outdoor electrical insulators are essential components of the power grid since they provide mechanical support to the high voltage carrying conductors besides the intended electrical insulation. Since insulator breakdown is a leading cause of electrical failure, precise information about the insulator surface condition is crucial and is of a high priority. The performance of outdoor insulators is often affected by atmospheric pollution, aging, and severe weather conditions (humidity, icing, heat, dust, ultraviolet) [1]. To prevent the faults in insulators, power grid operators have to conduct regular visual condition monitoring.

Insulator inspection methods, which are extensively used, include standard ground patrolling, and airborne imaging through helicopters. During these procedures, the power lines

The associate editor coordinating the review of this manuscript and approving it for publication was Wentao Fan.

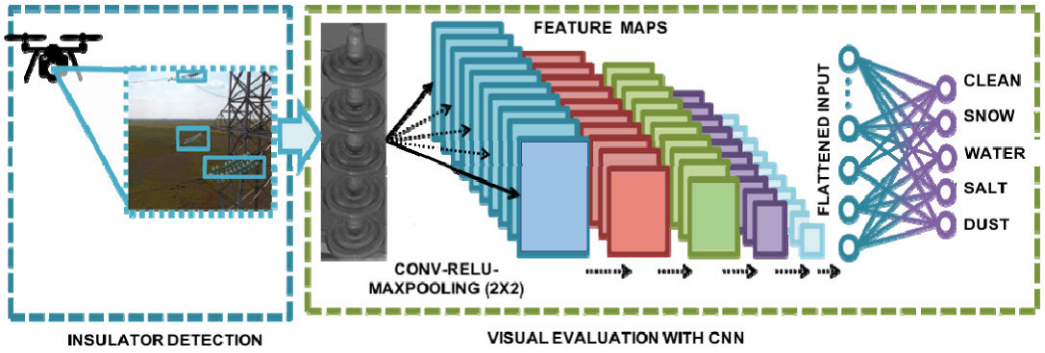

FIGURE 1. Deep CNN architecture for the classification of insulator surface contaminations.

and their components are observed using optical measuring devices [2], [3]. Ground patrolling inspectors perform the visual inspection using different instruments, such as, binoculars, infrared radiation, and ultraviolet (UV) cameras, and identify external defects and the pollution intensity on the outdoor insulators. While these approaches are practical, the work involved is too cumbersome since a large number of insulators, placed in geographically isolated remote locations, are to be inspected during extreme weather conditions. To overcome these challenges and improve the conventional monitoring methods, different remote sensing techniques, employing a variety of platforms (unnamed aerial vehicles, satellites, etc.), have been proposed and applied for the condition monitoring of electrical insulators [4].

Recently, the use of unmanned aerial vehicles (UAVs) has shown potential in airborne imaging for the surveillance of the power lines apart from other applications [5]. The benefits of employing UAVs include, mobility, low operating costs, and the possibility of computer vision with the aid of online edge computing. It is likely to achieve higher accuracies of detection and classification of outdoor objects using computer vision on edge devices enabled with deep learning CNN algorithms [6]. The overall framework of UAV deployment to enable visual inspection and analysis of insulators with the help of CNN algorithms is illustrated in Figure 1. However, owing to the resource constraints of small-scale commercial UAVs, implementation of this scheme requires immense computing and communication-related operations, making this a challenging task [7]. Currently, the implementation of onboard machine learning algorithms to the UAV devices for embedded scenarios is one of the leading research directions for edge computing [8], [9], communication [10], [11], and cloud computing fields [12]. In this article, we propose to reduce the computational overhead of the computer vision algorithms to facilitate edge processing on UAV devices. In the proposed work, this is achieved by minimizing the trainable parameters of CNN and compensating the architecture reduction with information fusion approach. The novel architecture, referred here as Fusion Convolutional Network (FCN), is found to be less time-consuming and has low memory requirements compared to the state-of-the-art deep learning architectures and conventional machine learning (ML) algorithms on the same dataset classification tasks. FCN uses multi-modal information fusion (MMIF) of drone images with the insulator surface leakage current values (LCV) and classifies insulator contamination into the states that usually precede failures such as, water, snow, metal dust, and salt.

To elaborate implementation of the proposed Fusion Convolutional Network approach and establish its efficacy, the following tasks are carried out and discussed in various sections and sub-sections of the manuscript.

1) Development of the image dataset comprising of five classes of outdoor insulators acquired *via* a drone under real winter condition. (sub-section III a)
2) Experimental measurement of the leakage current data, that correspond to the types of the pollutant on the insulator surface. (sub-section III b)
3) Construction of MMIF dataset, using NN encoding, and feature extraction techniques. (Section IV)
4) Training of FCN using the MMIF dataset of LCV and the images. (Section IV).
5) Comparison of FCN performance with conventional ML algorithms such as IBK, SMO, SVM, Random Forest, XGBoost, and Extra Trees on MMIF data, using different fusion techniques. (Section V)

II. METHODS

The technological advancements in UAV mechanisms, wireless sensing, and AI-based computing have put forth new opportunities for the deployment of possible real-time intelligent inspection of outdoor electrical insulators. Surveying, based on UAV imaging, has been successfully applied to diverse applications, such as agriculture [13], military [14], industrial plants [15], etc. Visual monitoring of the power transmission systems can also be efficiently carried out using UAVs, owing to their high mobility, low operating cost, and ability to access obscure, intricate, and remote areas. Airborne inspection of high-voltage lines will also save the personnel from potential hazards and inconvenience. Various methods used in this research are discussed in the following subsections.

A. IMAGE DATA ACQUISITION

For image data acquisition, the UAV equipped, with a camera sensor, was flown over the high voltage insulators inside the Nazarbayev University campus. The initial database, consisting of aerial images of a glass insulator, was acquired from the UAV during the winter season. The insulator creepage surface was artificially contaminated using dust, snow, sea-salt, and water and captured using a UAV mounted sensor. The database was further augmented using four types of noise such as the Gaussian, the Salt and Pepper, the Poisson, and the Speckle noise. While the Gaussian noise was used to mimic several independent environmental factors occurring naturally, the Salt and Pepper noise was added to represent the sharp and sudden disturbances in the image signal. The Speckle noise, on the other hand, characterizes an inherent granular interference that degrades the images captured. The augmented datasets, composed of 1000 initial and 4000 filtered images of the glass insulator, was labelled with five classes. The four labelled classes were, dust, snow, sea-salt, and water on the insulator surface, whereas the fifth class was for images of clean insulator surface. Each class consisted of 1000 images with 254 $\times$ 103 pixels resolution. The database was further split into train and testing databases. Samples of the filtered images are shown in Figure 2.

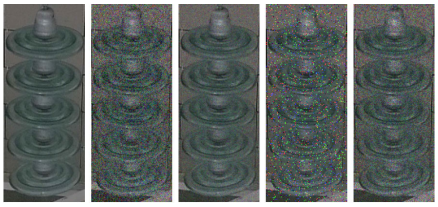

FIGURE 2. Image samples of a glass insulator: (a) original image (b) Gaussian, (c) Poisson, (d) Salt and Pepper, and (e) Speckle noise.

B. IMAGE CLASSIFICATION USING ML ALGORITHMS

Visual monitoring of high voltage insulators was carried out to classify various surface contaminations such as water, snow, metal dust, and salt. Conventional Machine learning algorithms were implemented for this purpose. The algorithms employed are namely, Naive Bayes, Sequential Minimal Optimization (SMO), IBk or k-NN, and J48. Insulator evaluation using these shallow classifiers shows moderate performance, reportedly reaching up to 90.05% accuracy [17], [18] on fault detection tasks. Later, more advanced classifiers, namely, SVM, Random Forest, XGBoost, and Extra Trees were also implemented, and improved accuracy was recorded. However, the use of these classifiers is criticized for being time and memory consuming and calls for optimization of algorithms and data processing [19].

C. CONVOLUTIONAL NEURAL NETWORKS

Convolutional Neural Network (CNN) is a biologically inspired neural network widely used for image processing and has shown to be valuable particularly for vision-based applications. The benefits of using CNN are derived from its structure, which is robust to translation, scaling, and tilting transformations. Given the fact that such transformations were presented in the present training dataset, CNN can be a suitable candidate for data analytics. CNN also allows the sharing of weights for both feature extraction and classification within a single architecture. A typical CNN architecture comprises of multiple convolutions and pooling layers for feature extraction, followed by fully connected dense layers for classification. Convolution refers to the process of sliding a filter mask (weights) or kernel over the input images by executing simple matrix multiplication resulting in a feature map as an output. Multiple filters are trained to learn and detect specific patterns in the images. The main purpose of applying pooling layers is to reduce the size of feature maps preserving meaningful information and increase the robustness of the model to affine and perspective transformations. The fully connected layer or the dense layer, on the other hand, performs simple classification on feature maps.

CNN, therefore, are state-of-the-art models for all image tasks including, image generation, classification, recognition, object detection, and segmentation. There are modern deep CNN architectures such as, InceptionV4 [20], MobileNet version 3 [21], VGG [22], and ResNet50 [23], that are proven to be effective techniques for image data analytics. These networks provide high classification accuracy on large datasets, such as ImageNet, and are known for their complex structures. A comparison of popular modern CNN structures is provided in Table 1, indicating the number of convolution layers, dense layers, number of kernels, and trainable parameters (weights).

In the present research, UAV based image processing for the insulator localization and its surface detection has been carried out using state-of-the-art CNN algorithms such as SSD [24], Yolo9000 [25], Faster RCNN VGG16 [26], Faster RCNN [27] and detection problems [5], [28], [29].

D. INSULATOR INSPECTION AND INFORMATION FUSION

Machine learning algorithms may not be the best candidates to provide higher accuracies in the present case of insulator inspection owing to certain limitations. Some of these constraints are the small size of training data, data imbalance (disproportionate instances of the classes), cluttered backgrounds, and non-uniform illumination. Therefore, it is proposed to consider the integration of multimodal information fusion to enhance the accuracy of classification. Multimodal information fusion (MMIF) methods are applied to facilitate decision making from different types of data obtained from multiple distributed sources. Information fusion techniques are used in different multisensory applications such as image fusion for detection and recognition [30], smart city domains [31], biometric systems [32], UAV systems [33], etc. There are a few studies that report the use of fusion approaches applied to the insulator pollution detection

TABLE 1. Comparison of state-of-the-art CNN architectures.

Metric	InceptionV3	MobileNet	VGG16	ResNet50	ResNeXt101	proposed CNN
Input size	3× 103×254	3× 103×254	3×103×254	3×103×254	3×224×224	3×103×254
# of CN layers	12	13	5	53	5 (32 groups)	5
Depth in # of CN layers	2	5	13	49	101	32
Filter sizes in CN layers	3, 5 ,1	3,5,11	3	1,3,7	7,1,3	3
# of channels in CN layers	1, 20	3-256	3-512	3-2048	4,4,256	3
# of filters in CN layers	32,64,80, 192	96-384	64-512	64-2048	128,256,512	32, 32, 32, 32, 64
Parameters in CN layers	2.6K	2.3M	14.7M	23.5M	48.96M	47.2K
Total parameters	24.1M	3.4M	15.4M	21.4M	87M	72.1K

tasks. During previous such studies [34], [35], multispectral fusion using visible light, infrared and ultraviolet images of insulators was proposed to improve the accuracy of image detection of the contaminated insulators and discriminate insulator contamination grades. However, the fusion of multisource images [36] was not able to improve the detection accuracy rate beyond 90%. In the present work, the leakage current data is proposed to be combined with the insulator image data to increase the inspection accuracy of outdoor insulators.

III. EXPERIMENTAL SETUP AND DATASET

A. INSULATOR IMAGES

The image dataset was captured using DJI Mavic II, powered by a mirrorless camera system of 1/2.3-inch ($6.17 \times 4.55mm$), a 12-megapixel sensor. The insulator surface, artificially contaminated with dust, snow, sea-salt, and water was captured, and the image data (Figure 2) was augmented as discussed in the previous section. The data is divided into training and testing datasets in a proportion of 90% and 10% respectively. Later, the training dataset was subjected to ten-fold cross-validation, whereby, nine subsets were used for training, and the remaining one was used for validation purposes. A generalization capability of the model was evaluated on the test sample by implementing the L2 regularization approach.

B. LEAKAGE CURRENT MEASUREMENT

Leakage current (LC) from the insulators is an indicative sign of the unsatisfactory performance of insulators. The leakage of current, from insulators, adversely affects the stability and the reliability of the power grid [37]. Therefore, leakage current values are considered as crucial information, that can be used to monitor the performance of contaminated insulators [38].

In the present work, surface leakage current values of insulators are obtained in the laboratory conditions using an injection test system called CPC100-Omicron®. Multiple leakage current measurements were conducted applying 5 kV across the glass insulators with different types of contamination: water, salt, snow, and metallic dust. For each of the contamination types, 20 experiments were performed, and 18 leakage current values were recorded (after removing noise). Leakage current values, for various contaminations on the insulator surface, are provided in Fig. 3.

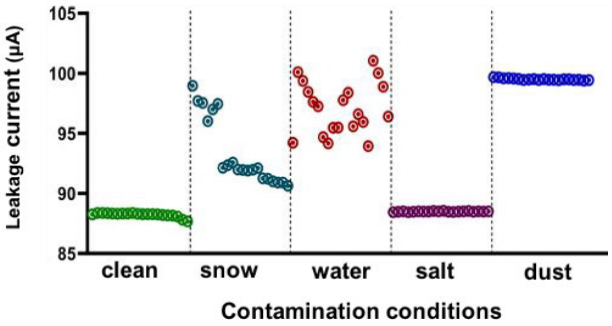

FIGURE 3. Leakage current values for different contaminations conditions.

IV. FUSION CONVOLUTIONAL NETWORK (FCN)

The novel Fusion Convolutional Network (FCN) architecture for classification of contamination types on electrical insulators is proposed in this research. The classification is performed on five surface conditions of the insulator, namely, clean and contaminated with water, snow, metal dust, and salt. In the proposed FCN architecture, a deep convolutional neural network (CNN) and multilayer neural networks (MNN) are combined to achieve higher classification accuracy. The architecture of this algorithm is implemented in two-stages. During the first stage, the aerial images of insulators and leakage current values (LCVs) are encoded to the same modality. In the second stage, a fusion of this data is used as a series of inputs to the network of sub-classifiers. The architecture of the proposed FCN is shown in Figure 4, whereby it is seen that the images are fed to CNN, while the set of LCV measurements is encoded with MNN. The fusion of CNN and MNN outputs (X_{CNN} *and* x_i respectively) is used as the input to the network of independent MNN subclassifies (MNN_{1-5}). Sub-classifiers are responsible for the final image classification.

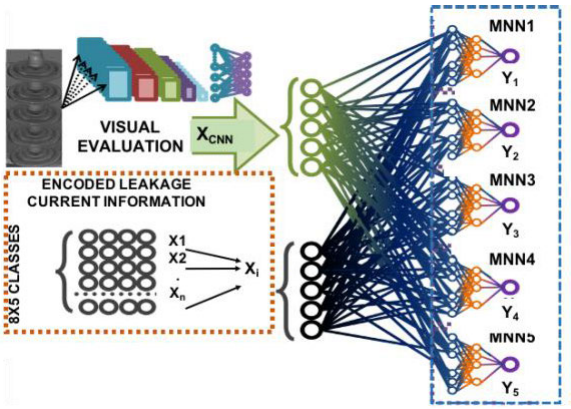

FIGURE 4. Information fusion for electrical insulator inspection based on fusion convolution network.

A. PROPOSED FCN ARCHITECTURE

The proposed network scheme evaluates insulator surface conditions in two stages. First, the visual information is processed with a CNN and then the results from CNN are improved employing the FCN. The enhancement of the CNN accuracy is achieved using the fusion of probability spaces resulting from two types of information, namely, the visual classification and encoded leakage current information as shown in Figure 4. The implementation of the proposed FCN scheme is further explained using pseudocode in Table 2. Lines 3 to 11, in the Pseudocode, present the training of CNN to classify the contamination type on detected insulator images (explained further in the next subsection). Concurrently, the online measurements of LCVS, from the insulator, are required to be fed to the MNN which is trained to recognize the contamination type using LCVs. However, online translation of surface leakage current measurements of insulators is still open to research [39], [40]. Therefore, in the present work, pre-measured LCVs (experimental measurements, $18 \times 5 = 90$) were used and encoded with the MNN. In other words, instead of online encoding of LCVs, the dataset of pre-encoded LCVs, (x_{1-90}) were combined with the current output of CNN (X_{CNN}) (lines 18-20 in pseudocode, Table 2). As a result, all samples of the encoded LCV dataset will be combined with the present CNN output to construct the series of fusion samples, i.e. ($X_{CNN} \mid x_i$) or $F[f_{1-90}]$. The series of fused data F will be the common input for all the five sub-classifiers of the FCN (MNN_{1-5}).

Each sub-classifier is trained to recognize one of the insulator contamination types, in such a manner, that MNN_1 recognizes clean insulator surface while, MNN_{2-5}, recognize water, snow, metal dust, and salt contaminations, respectively.

During the second stage (lines 23-29 in pseudocode, Table 2), the MNN sub-classifiers perform binary classification on each sample $[f_{1-90}]$ in F. Sub-classifier that accumulates the greatest number of positive predictions in the fusion series determines the final class of the fusion (explained in the next subsection).

TABLE 2. FCN Algorithm Pseudocode.

Fusion Convolutional Network
1: Stage I: Convolutional Neural Network (CNN)
2: **A** Feature extraction:
3: **for all** j input image matrix, size (103, 254) **do**
4: Convolution with kernel filter (32, 3 × 3)
5: Activation with ReLU
6: Max-pooling (2 × 2)
7: Convolution with kernel filter (64, 3 × 3)
8: Activation with ReLU
9: Max-pooling (2 × 2)
10: **end for**
11: Output: Feature maps
12: **B** Classification:
13: Input layer: Flatten (Feature map)
14: Hidden layer: (64, Activation [ReLU, Softplus])
15: Output: X_{CNN}
16: Information fusion:
17: **for all** x_i in X: **do**
18: $F = CONCAT(X_{CNN}, x_i)$
19: **end for**
20: Output: F of the size [90 × 10]
21: Stage II: Fusion network:
22: **for all** i in F
23: $y_i^1 = MNN_1()$
24: $y_i^2 = MNN_2()$
25: $y_i^3 = MNN_3()$
26: $y_i^4 = MNN_4()$
27: $y_i^5 = MNN_5()$
28: **end for**
29: Output: Predicted class of
$y_i = max(\sum y_1, \sum y_2, \sum y_3, \sum y_4, \sum y_5)$

1) CNN ARCHITECTURE

The architecture of the CNN, used here, comprises an input layer, five convolutional layers, and two Dense layers (Figure 1). The first layer of the network takes the image of size 254 × 103 × 3 as an input vector. The following layers are the sequence of multiple convolutional and pooling layers that reduce the input size to 64 × 6. The kernel size of convolutions was kept as 3 × 3 throughout the network and the pooling size was kept as 2 × 2. Table 1 provides input and output sizes of each layer, the number of the kernel, and trainable parameters of the CNN implemented.

During this research, different combinations of activation functions and optimization routines were tested in order to achieve the best performance of CNN. Using Adadelta as an optimizer, Softplus as an activation function for the dense layer, and mean squared error (MSE) as a loss function, resulted in the highest validation accuracy of the proposed CNN. A brief introduction of these tools is given here for a quick reference.

- Adadelta is an optimizer, based on the adaptive learning rate per dimension, widely used to modify the weights and minimize the loss during the network training. It utilizes different learning rates η at each time step t for every parameter θ. It restricts the window of previous gradients to a fixed size. The formulation for Adadelta

used here is defined as (1).

$$\Delta\theta_t = -\frac{RMS[\theta_t]_{t-1}}{RMS[g]_t} \cdot g_t \tag{1}$$

where $\Delta\theta_t$ is the parameter update vector; RMS refers to the root mean squared error; θ_t is the updated parameter variation; g_t is the gradient of the stochastic gradient descent algorithm.

- The activation function used for the last dense layer is SoftPlus, which is a smooth approximation to ReLU (2).

$$f(x) = \log(1 + e^x) \tag{2}$$

- Mean square error (MSE) is one of the most widely used loss functions, which averages the squared differences between the actual value and predicted value (3).

$$Loss(x, y) = 1/n \sum |x_i - y_i|^2 \tag{3}$$

2) MULTI-MODAL INFORMATION FUSION OF CNN-MNN OUTPUTS

In order to combine the CNN predictions X_{CNN}, with the pre-measured LCVs (x_i), into MMIF dataset of F fusion series, a set of pre-encoded LCVs $X[x_{1-90}]$ was created using the MNN algorithm. We use three consequent data points from each class of leakage current measurements to form a single sample of encoded LCV (x_i). There are 18 encoded samples for LCVs per class and therefore all the given measurements were encoded into 90 vectors. Encoding operation was performed with the simple three-layer MNN. This MNN contains an input layer with the size 1×3, hidden layer dimension is 1×12 and an output layer of 1×5 size which is equal to the number of classes. To preserve the information modality with X_{CNN}, the last layer of MNN is activated with Softplus, and the hidden layer is activated with ReLU. The MNN was trained to map the contamination type of the insulator to five classes of pre-measured LCVs and was used to encode them into vectors $X[x_{1-90}]$ compatible with X_{CNN} modality.

3) FCN AND VOTING

Fusion Convolutional Network consists of 5 independent MNN sub-classifiers (MNN_{1-5}) as shown in Figure 4. The input of the FCN is a 10-dimensional vector which comprises of two vectors, the CNN output X_{CNN}, and pre-encoded LCV (x_i). All the sub-classifiers are of the same size, and each of these is responsible to recognize only one class, making this a binary classification problem. While the input for all sub-networks is common, each (MNN_i) is trained separately.

As the proposed CNN is already trained on training sets of images, the validation set of images is used to collect CNN predictions that were further fused with pre-encoded LCVs to train FCN. Thus, the training dataset of MNN sub-classifiers includes a fusion of CNN predictions on unseen images with pre-encoded LCVs. Each of the training MMIF dataset samples consists of fusion series $F[f_{1-90}]$ that has the size of 90×10, where each f_i is the concatenated X_{CNN} and x_i from $X[x_{1-90}]$ (lines 18-20 in pseudocode, Table 2).

While sub-classifiers are trained on common inputs, each sub-classifier has its own set of labels to be used for supervised learning. The network of sub-classifiers (MNN_{1-5}) has to classify all f_{1-90} in sample F to output the classification result. The output of the FCN, therefore, will be the class of MNN_i that has the highest number of positive predictions on $F[f_{1-90}]$. This process can be referred to as the majority voting since we predict the final class label with the class label of MNN_i that gave the positive prediction most frequently.

About the structure of the sub-classifiers, each MNN has layers of the size 1×10, 1×15, 1×7 and 1×1. During training, the MNN sub-classifiers were examined for different activation functions. The activation functions finally selected were, Sigmoid, Softmax, and Relu for first, second, and output layers. The activation functions of the first layer of subnetwork MNN_4 was altered to ReLU to enhance its performance. The higher accuracy was achieved using Stochastic Gradient Descent (SGD) optimization and MSE loss function. Activation functions and voting used are further explained here.

- A Sigmoid function is the special case of a logistic function that have of all real numbers between 0 and 1, and known in statistics as cumulative distribution function:

$$f(x) = \frac{1}{1 + e^{-x}} = \frac{e^x}{e^x + 1} \tag{4}$$

- The standard (unit) softmax function, $\sigma : \mathbb{R}^K \to \mathbb{R}^K$ also known as annmmfyftygftgwstge3gfveg normalized exponential function, is defined by (5).

$$f(x)_i = \frac{e^{x_i}}{\sum_j^k e^{x_j}} \tag{5}$$

For $i = 1, \ldots, K$ and $x = (x_1, .., x_K) \in \mathbb{R}^K$
The FCN outputs can be defined as below.

$$Y_i = \begin{cases} 1, & if\ max\ (f(x_1), f(x_2), \ldots, f(x_5)) \\ 0, & otherwise \end{cases} \tag{6}$$

B. FEATURE EXTRACTION FOR FCN ARCHITECTURE

To test the majority voting classification method on conventional classifiers, besides FCN, additional feature extraction approaches were applied. The Wavelet transform and the Principal Component Analysis (PCA) were selected to reduce the dimensions of the image and LCV datasets for the classification process.

C. ENCODING WITH WAVELET TRANSFORM

The Wavelet transform (WT) is a widely applied feature extraction technique used for the reduction of dimensionality of data by selecting a band of wavelet coefficients [41]. There are several functions that can be used for Wavelet Transformation. In the present work, the Haar wavelet function was chosen, owing to its wide applications in image processing [42]. Haar wavelet uses a sequence of rescaled square-shaped functions to form a wavelet family. This analysis is quite similar to the Fourier analysis whereby a target

function is represented in terms of an orthonormal basis over a given interval. Three-level Haar transforms were performed on each of the images and 5 data-points from LCV measurements. Standard deviation, and mean values for each extracted vector were calculated, resulting in 8 coefficients from image pixels and 2 coefficients from LCV measurements. Fusion of this data into a 10-dimensional input vector is performed as instructed in lines 18-20 in the pseudocode in Table 2.

1) ENCODING WITH PCA COEFFICIENTS

Principal component analysis [43] is a technique for reducing the dimensionality of data preserving the meaningful information. The selection of principal components is performed using singular decomposition of the covariance matrix of the original data. In the present work, as a consequence of PCA analysis, 8 principal components were chosen from the image matrix, while 2 components were selected from the LCV measurements (5 data-points each). Later, this data was fused into the 10-dimensional input vector.

V. RESULTS AND DISCUSSION

To begin with, the results of the experiments with shallow classifiers and CNN models on the insulator images are provided in this section. Subsequently, classification results of the MMIF data, as a consequence of the implementations of CNN and FCN, respectively, are also provided here. Image classification performances of competing CNN architectures such as VGG16, MobileNet, ResNet, ResNext101 and Inception are included for the sake of complete discussion (Fig. 6a). MobileNet and Inception architectures exhibit good efficiencies than the accuracies and are deserving candidates for real-time applications owing to the use of an optimal number of parameters. However, in the present application of the condition monitoring of insulators, where an on-line analysis may not be warranted, accuracy is preferred over efficiency.

Classification accuracies of various shallow algorithms, namely, SVM, Random Forest, XGBoost, and Extra Trees are provided in Figure 6b. Performances of classifiers were tested on the image data, extracting features via wavelet transform, principal component analysis techniques, and through the information fusion based on the CNN and MNN models.

A. IMAGE CLASSIFICATION

Proposed CNN was trained to classify the 5 types of insulator conditions with different optimization algorithms using the images from the training dataset. The best performance on the validation dataset, achieved with Adadelta optimizer and MSE loss function, was 92.12% of the classification accuracy. CNN performance is shown using a Receiver operating characteristic (ROC) plot in Figure 5. ROC curve shows a possible trade-off between accuracy and error rates for the given class and provides a single-value summary (ranging from 0 to 1). As it can be seen from the plot, that the misclassification is observed mostly in 2-salt and 4-metal dust classes with fewer recognition rates. To compare the performance

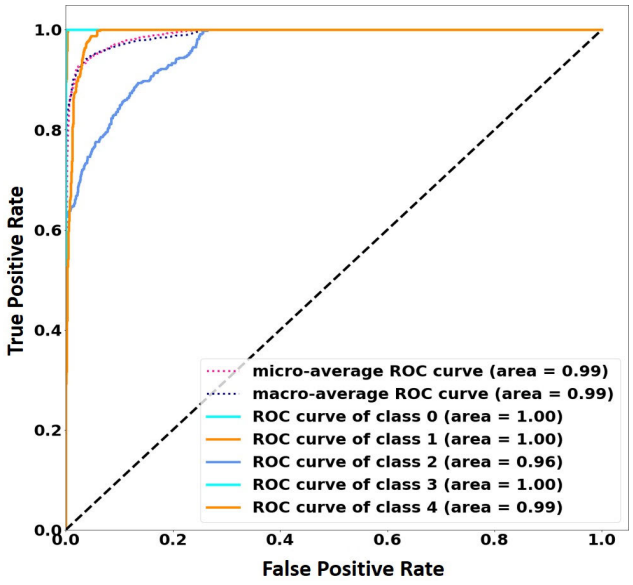

FIGURE 5. Receiver operating characteristic (ROC) curve of CNN categorical classification performance.

of proposed CNN with competing architectures, we further trained VGG16, MobileNet, InceptionV3, ResNeXt101 and ResNET50 using transfer learning that resulted in lower accuracy after 50 training epochs. Figure 6a shows the validation and training accuracy of the CNN architectures, indicating a possible over-fitting, which can be avoided employing suitable optimizers. On the other hand, less complex architecture structures used in the proposed CNN show faster training and less over-fitting. The performance of conventional machine learning algorithms with the varying success of classification on the validation data is shown in Figure 6b. IBK stands out with the highest accuracy at the validation stage, but at the same time, shows the highest memory and time usage for the same operation compared to the rest (Table 3). Table 3 further shows that IBK has the most significant memory allocation compared to the conventional ML algorithms and MobileNet from CNN architectures, while VGG16 and IBK are the slowest to perform predictions. It can be concluded here that the proposed CNN uses less memory and operates faster at the inference stage.

B. CLASSIFICATION OF MMIF

The memory and time usage for fusion classification and voting stages for conventional ML algorithms and FCN are also shown in Table 3. For the three types of fusion instances (CNN-MNN outputs, WT, and PCA), maximum memory allocation was required during feature extraction and while fusing with PCA. Similarly, the least memory was allocated during WT. The fastest feature extraction and fusion processes were recorded during WT and CNN-MNN feature fusions. At the classification level, SMO and FCN provided the fastest predictions, while the voting stage required the same memory and time allocation for each classifier. Overall,

TABLE 3. Memory usage and Time consumption of implemented classifiers.

Sub-Classifiers											
Features	Fusion	IBk	J48	Naive Bayes	SMO	FCN	VGG16	ResNet50	MobileNet	Inception	Voting
PCA mem. usage, MiB	99.8	269.89	644.7	578.9	1381.9	-	-	-	-	-	1.43
PCA time consumed, Sec/sample	0.042	0.56	0.002	0.0025	0.002	-	-	-	-	-	0.026
WT (haar), mem. usage, MiB	0.20	302.32	430.12	502.59	342.37	-	-	-	-	-	1.43
WT (haar), time consumed, Sec/sample	0.171	0.53	0.004	0.01	0.024	-	-	-	-	-	0.026
CNN-MNN, mem. usage, MiB	4.29	254.63	158.31	262.26	189.78	0.4297	-	-	-	-	1.43
CNN-MNN, time consumed, Sec/sample	0.04	0.009	0.008	0.016	0.009	0.001	-	-	-	-	0.026
Classifiers											
Raw Image	Fusion	IBk	J48	Naive Bayes	SMO	CNN	VGG16	ResNet50	MobileNet	Inception	-
Mem. usage, MiB	-	1286	1193.05	655.174	765.8	0.417969	19.2	19.2	36.8	19.2	-
Time consumed, Sec/sample	-	0.96	0.0064	0.026	0.009	2.4e-06	0.55	0.10	0.45	0.38	-

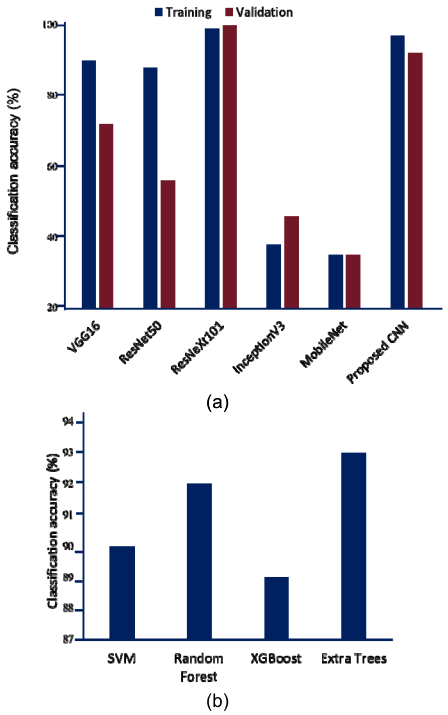

FIGURE 6. Classification accuracy based on images pixels employing (a) state-of-the-art CNN models vs. proposed CNN and (b) ML classifiers.

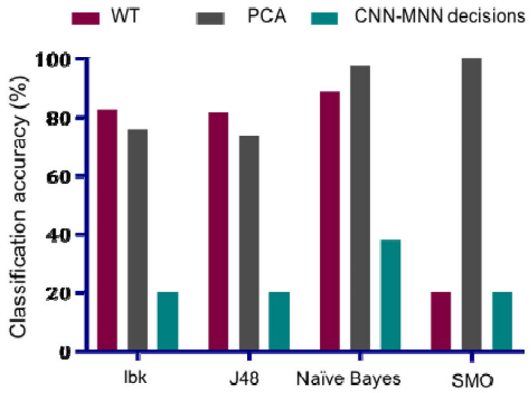

FIGURE 7. Classification accuracy of traditional ML algorithms using different features: CNN-MNN based decisions, wavelet transform (WT), principal component analysis (PCA).

FCN classification shows the least time consumption and memory usage for a single prediction.

The accuracy of the trained FCN was observed to be 99.76%, enhancing the performance of CNN (92.12%) considerably. Figure 7 shows the low performance of classifiers (from 20-38%) that used the decisions of networks based on MMIF. The reason for the low performance could be that the data was not enough and was sparse for proper training of the classifiers. Classification accuracy based on the raw images was high with IBk classifier, while others performed in the range of 54-80 %. J48 and Naive Bayes show improvement in accuracy using WT and PCA features. Although ML classifiers show relatively good classification accuracy but compared to the deep learning models, they are computationally expensive and require hand-coded data preparation and feature extraction. fusing with PCA.

As the system-level simulations of FCN showed high classification performance, we further analyzed a possible hardware implementation of FCN for an embedded scenario of airborne imaging.

C. FCN HARDWARE

Since the target of this work is to propose methods for enhanced CNN classification of insulators with MMIF approach, there is a perspective of implementing such a system on hardware with emerging technologies such as analog resistive memories, i.e. memristors [44]. The potential implementation of different architectures such as NN, CNN, and

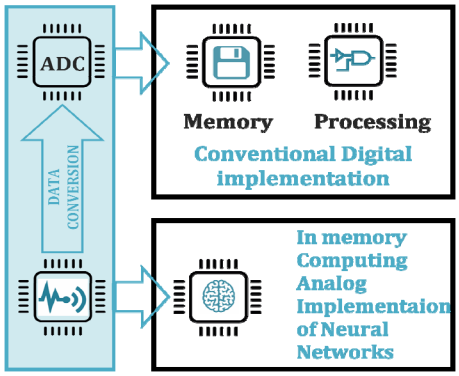

FIGURE 8. Hardware implementations of FCN System on digital and analogue domains.

LSTM was previously proposed successfully [45]. Successful implementation of such systems depends how best the memory analog dot product computing scheme can be exploited. The definition of the memristors suggests a possibility of continuous analogy memory implementation while the fault rate of the technology is still high. Figure 8 shows two possible approaches, digital and analog for the implementation of such a system hardware. The selection of either approach can be justified with the benefits of the respective technology.

Recent advances in the digital technology also affects the potential efficacy of analog architectures. Implementing the FCN system on mature digital technologies will guarantee the accuracy of the stored synaptic weights and computing logic operations. However, this will require more chip areas with built-in analog to digital conversion blocks, separate data processing, and data storage blocks that may affect the communication bandwidth as well. Analog implementation of neural networks can be integrated on sensor backplanes to work directly with analog signals for memory dot product operation. This will save on-chip area and increase the speed of the decision-making process. Considering potential practical aspects of FCN implementation, we have conducted fault tolerance of digital and analog implementation of FCN memory. To use emerging memories as binary cells, we also considered the failure scenario for the digital implementation of the memory. Three cases of memory faults were analyzed:

1) The analog value of the stored synaptic weight is up to, $\pm\sigma^1$

$$\sigma_i^1 = rand(0, \frac{2\,|\mu \pm \sigma|}{3k}) \tag{7}$$

Here, μ is the average synaptic value of FCN, σ stands for the standard deviation of synaptic values of FCN, and k is used for the number of analog levels.

2) The analog value of the stored synaptic weight is up to $\pm\sigma^2$

$$\sigma_i^2 = rand(0, \frac{w_i}{k}) \tag{8}$$

Here, i is the iterator, and w is used for synaptic weight values.

3) The binary 32 bit representation of the floating synaptic weight value has random flipped bits (reversed from 0 to 1, from 1 to 0) across the FCN.

Figure 9 shows the performance of FCN in the above three different cases. It can be noticed that the variation in the analog implementation of the FCN memory has less impact on the accuracy of the system when the number of levels reaches about 32 and higher. Contrary to this, the digital implementation of FCN memory starts to fail with only 100 bits flipped in the system, provided that there are 7542 synapses stored in 32bit format. It should be noted that the failure of random memory cells that store synapse bits, may result in extremely high or low values, depending on the significance of the bit if not set correctly.

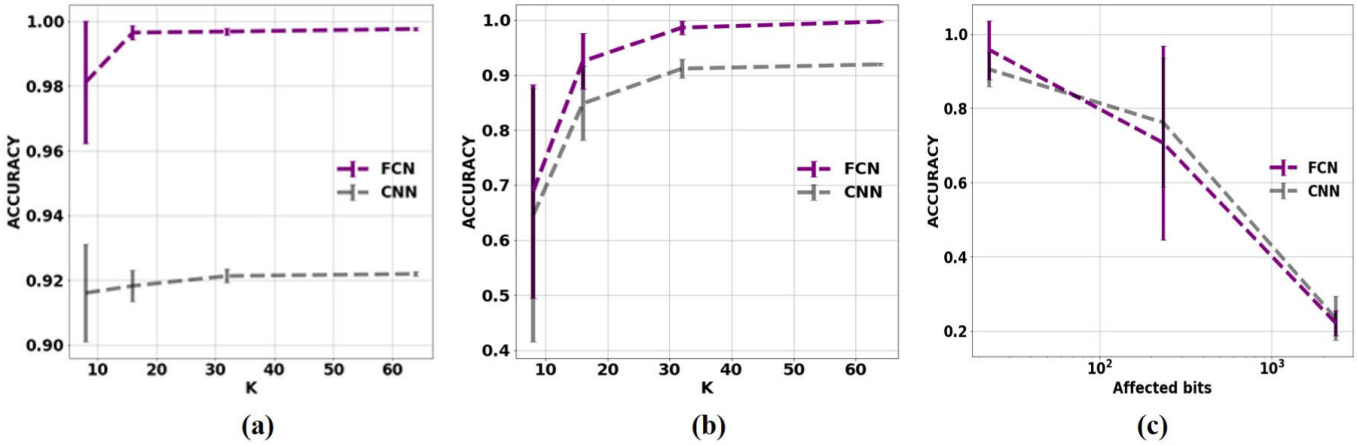

FIGURE 9. Three cases of memory faults: (a)The analogue value of the stored synaptic weight has up to $\pm\sigma^1$ (7); (b) the analogue value of the stored synaptic weight has up to $\pm\sigma^2$ (8); (c) the floating synaptic weight value has random flipped bits across the FCN.

VI. CONCLUSION

A Fusion Convolutional Network (FCN) architecture is proposed in this article for UAV-based remote evaluation of the contaminated outdoor high-voltage insulators. The proposed FCN is a multi-modal information fusion system, where the image data and the leakage current data were combined to achieve better accuracy for the classification of insulator surface contaminations. Five types of insulator surfaces were analyzed, namely, a clean surface, and surfaces contaminated with water, snow, metal dust, and salt. By employing the multi-modal information fusion approach, it was possible to reduce the complexity of the CNN structure, and at the same time, increase the classification accuracy from 92% to 99.76%. To benchmark, the FCN results with the existing approaches, traditional machine learning classifiers and competent CNN architectures were implemented and compared. Results from this comparison revealed that the proposed FCN system was able to provide higher accuracy of classification with less time and memory consumption.

Further, to assess the potential future applications of the proposed FCN in an embedded scenario, a hardware-oriented analysis was also performed. A fault tolerance analysis was carried out and the results, for both digital and analog FCN systems, were obtained and analyzed. It was found that the accuracy of the FCN system remains invariant to the inexorable aberrations, during the analog implementation of the FCN memory. Therefore, it is recommended that an analog implementation should be preferred over a digital implementation. In future research work, further studies shall be conducted with the perspective of the implementation of an on-chip FCN system integrated with the UAV camera sensor.

REFERENCES

[1] C. Zhang, L. Wang, Z. Guan, and F. Zhang, "Pollution flashover performance of full-scale ±800 kV converter station post insulators at high altitude area," *IEEE Trans. Dielectr. Electr. Insul.*, vol. 20, no. 3, pp. 717–726, Jun. 2013.

[2] J. Molina and S. Hirai, "Pruning tree-branches close to electrical power lines using a skew-gripper and a multirotor helicopter," in *Proc. IEEE Int. Conf. Adv. Intell. Mechatronics (AIM)*, Jul. 2017, pp. 1123–1128.

[3] Q. Guo and X. Hu, "Power line icing monitoring method using binocular stereo vision," in *Proc. 12th IEEE Conf. Ind. Electron. Appl. (ICIEA)*, Jun. 2017, pp. 1905–1908.

[4] L. Matikainen, M. Lehtomäki, E. Ahokas, J. Hyyppä, M. Karjalainen, A. Jaakkola, A. Kukko, and T. Heinonen, "Remote sensing methods for power line corridor surveys," *ISPRS J. Photogramm. Remote Sens.*, vol. 119, pp. 10–31, Sep. 2016.

[5] X. Tao, D. Zhang, Z. Wang, X. Liu, H. Zhang, and D. Xu, "Detection of power line insulator defects using aerial images analyzed with convolutional neural networks," *IEEE Trans. Syst., Man, Cybern. Syst.*, vol. 50, no. 4, pp. 1486–1498, Apr. 2020.

[6] M. Z. Khan, S. Harous, S. U. Hassan, M. U. G. Khan, R. Iqbal, and S. Mumtaz, "Deep unified model for face recognition based on convolution neural network and edge computing," *IEEE Access*, vol. 7, pp. 72622–72633, 2019.

[7] W. Chen, B. Liu, H. Huang, S. Guo, and Z. Zheng, "When UAV swarm meets edge-cloud computing: The QoS perspective," *IEEE Netw.*, vol. 33, no. 2, pp. 36–43, Mar. 2019.

[8] J. Kok, L. F. Gonzalez, and N. Kelson, "FPGA implementation of an evolutionary algorithm for autonomous unmanned aerial vehicle on-board path planning," *IEEE Trans. Evol. Comput.*, vol. 17, no. 2, pp. 272–281, Apr. 2013.

[9] L. Zhang, Z. Zhao, Q. Wu, H. Zhao, H. Xu, and X. Wu, "Energy-aware dynamic resource allocation in UAV assisted mobile edge computing over social Internet of vehicles," *IEEE Access*, vol. 6, pp. 56700–56715, 2018.

[10] G. H. S. Carvalho, I. Woungang, A. Anpalagan, and M. Jaseemuddin, "Analysis of joint parallelism in wireless and cloud domains on mobile edge computing over 5G systems," *J. Commun. Netw.*, vol. 20, no. 6, pp. 565–577, Dec. 2018.

[11] T. Taleb, K. Samdanis, B. Mada, H. Flinck, S. Dutta, and D. Sabella, "On multi-access edge computing: A survey of the emerging 5G network edge cloud architecture and orchestration," *IEEE Commun. Surveys Tuts.*, vol. 19, no. 3, pp. 1657–1681, 3rd Quart., 2017.

[12] B. P. Rimal, D. P. Van, and M. Maier, "Mobile-edge computing versus centralized cloud computing over a converged FiWi access network," *IEEE Trans. Netw. Service Manage.*, vol. 14, no. 3, pp. 498–513, Sep. 2017.

[13] A. Tewes and J. Schellberg, "Towards remote estimation of radiation use efficiency in maize using UAV-based low-cost camera imagery," *Agronomy*, vol. 8, no. 2, p. 16, Feb. 2018.

[14] N. Lissandrini, G. Michieletto, R. Antonello, M. Galvan, A. Franco, and A. Cenedese, "Cooperative optimization of UAVs formation visual tracking," *Robotics*, vol. 8, no. 3, p. 52, Jul. 2019.

[15] F. Mesas-Carrascosa, D. V. Santano, F. P. Porras, J. Meroño-Larriva, and A. García-Ferrer, "The development of an open hardware and software system onboard unmanned aerial vehicles to monitor concentrated solar power plants," *Sensors*, vol. 17, no. 6, p. 1329, Jun. 2017.

[16] I. H. Witten, E. Frank, M. A. Hall, and C. J. Pal, "The WEKA workbench online appendix," in *Data Mining: Practical Machine Learning Tools and Techniques*. San Mateo, CA, USA: Morgan Kaufmann, 2005.

[17] F. Guo, K. Hao, M. Xia, L. Zhao, L. Wang, and Q. Liu, "Detection of insulator defects based on YOLO V3," in *Proc. Int. Conf. Artif. Intell. Commun. Netw.*, 2019, pp. 291–299.

[18] S. Wang, L. Niu, and N. Li, "Research on image recognition of insulators based on YOLO algorithm," in *Proc. Int. Conf. Power Syst. Technol. (POWERCON)*, Nov. 2018, pp. 3871–3874.

[19] D. T. Nguyen, T. N. Nguyen, H. Kim, and H.-J. Lee, "A high-throughput and power-efficient FPGA implementation of YOLO CNN for object detection," *IEEE Trans. Very Large Scale Integr. (VLSI) Syst.*, vol. 27, no. 8, pp. 1861–1873, Aug. 2019.

[20] C. Szegedy, V. Vanhoucke, S. Ioffe, J. Shlens, and Z. Wojna, "Rethinking the inception architecture for computer vision," in *Proc. IEEE Conf. Comput. Vis. Pattern Recognit. (CVPR)*, Jun. 2016, pp. 2818–2826.

[21] A. G. Howard, M. Zhu, B. Chen, D. Kalenichenko, W. Wang, T. Weyand, M. Andreetto, and H. Adam, "MobileNets: Efficient convolutional neural networks for mobile vision applications," 2017, *arXiv:1704.04861*. [Online]. Available: http://arxiv.org/abs/1704.04861

[22] K. Simonyan and A. Zisserman, "Very deep convolutional networks for large-scale image recognition," 2014, *arXiv:1409.1556*. [Online]. Available: http://arxiv.org/abs/1409.1556

[23] K. He, X. Zhang, S. Ren, and J. Sun, "Deep residual learning for image recognition," in *Proc. IEEE Comput. Soc. Conf. Comput. Vis. Pattern Recognit.*, Jun. 2016, pp. 770–778.

[24] W. Liu *et al.*, "SSD: Single shot multibox detector," in *Proc. Eur. Conf. Comput. Vis.* Cham, Switzerland: Springer, 2016, pp. 21–37.

[25] J. Redmon and A. Farhadi, "YOLO9000: Better, faster, stronger," in *Proc. IEEE Conf. Comput. Vis. Pattern Recognit. (CVPR)*, Jul. 2017, pp. 6517–6525.

[26] G. Kang, S. Gao, L. Yu, and D. Zhang, "Deep architecture for high-speed railway insulator surface defect detection: Denoising autoencoder with multitask learning," *IEEE Trans. Instrum. Meas.*, vol. 68, no. 8, pp. 2679–2690, Aug. 2019.

[27] S. Ren, K. He, R. Girshick, and J. Sun, "Faster R-CNN: Towards real-time object detection with region proposal networks," *IEEE Trans. Pattern Anal. Mach. Intell.*, vol. 39, no. 6, pp. 1137–1149, Jun. 2017.

[28] H. Cheng, R. Chen, J. Wang, X. Liu, M. Zhang, and Y. Zhai, "Study on insulator recognition method based on simulated samples expansion," in *Proc. 30th Chin. Control Decis. Conf. (CCDC)*, Jun. 2018, pp. 2569–2573.

[29] G. Tao, C. Fengxiang, W. Wei, S. Ping, S. Lei, and C. Tianzhu, "Electric insulator detection of UAV images based on depth learning," in *Proc. 2nd Int. Conf. Power Renew. Energy (ICPRE)*, Sep. 2017, pp. 37–41.

[30] J. Ma, Y. Ma, and C. Li, "Infrared and visible image fusion methods and applications: A survey," *Inf. Fusion*, vol. 45, pp. 153–178, Jan. 2019.

[31] B. P. L. Lau, S. H. Marakkalage, Y. Zhou, N. U. Hassan, C. Yuen, M. Zhang, and U.-X. Tan, "A survey of data fusion in smart city applications," *Inf. Fusion*, vol. 52, pp. 357–374, Dec. 2019.
[32] M. Singh, R. Singh, and A. Ross, "A comprehensive overview of biometric fusion," *Inf. Fusion*, vol. 52, pp. 187–205, Dec. 2019.
[33] A. Nemra and N. Aouf, "Robust INS/GPS sensor fusion for UAV localization using SDRE nonlinear filtering," *IEEE Sensors J.*, vol. 10, no. 4, pp. 789–798, Apr. 2010.
[34] L. Jin, J. Ai, Z. Tian, and Y. Zhang, "Detection of polluted insulators using the information fusion of multispectral images," *IEEE Trans. Dielectr. Electr. Insul.*, vol. 24, no. 6, pp. 3530–3538, Dec. 2017.
[35] Z. Tian, L. Jin, Y. Zhang, J. Ai, C. Peng, and W. Duan, "Discrimination of insulator contamination grades using information fusion of multi-light images," in *Proc. IEEE 11th Int. Conf. Properties Appl. Dielectr. Mater. (ICPADM)*, Jul. 2015, pp. 967–970.
[36] L. Jin, J. Ai, Z. Tian, K. Gao, and H. Huang, "Pollution state detection of insulators based on multisource imaging and information fusion," in *Proc. IEEE Int. Conf. Dielectr. (ICD)*, Jul. 2016, pp. 544–547.
[37] Y. Liu, M. Farzaneh, and B. X. Du, "Nonlinear characteristics of leakage current for flashover monitoring of ice-covered suspension insulators," *IEEE Trans. Dielectr. Electr. Insul.*, vol. 23, no. 3, pp. 1242–1250, Jun. 2016.
[38] H. Yang, L. Pang, Z. Li, Q. Zhang, X. Yang, Q. Tang, and J. Zhou, "Characterization of pre-flashover behavior based on leakage current along suspension insulator strings covered with ice," *IEEE Trans. Dielectr. Electr. Insul.*, vol. 22, no. 2, pp. 941–950, Apr. 2015.
[39] J. M. de Barros Bezerra, A. M. N. Lima, G. S. Deep, and E. G. da Costa, "An evaluation of alternative techniques for monitoring insulator pollution," *IEEE Trans. Power Del.*, vol. 24, no. 4, pp. 1773–1780, Oct. 2009.
[40] J. Wang, Y. Xi, C. Fang, L. Cai, J. Wang, and Y. Fan, "Leakage current response mechanism of insulator string with ambient humidity on days without rain," *IEEE Access*, vol. 7, pp. 55229–55236, 2019.
[41] P. S. Addison, *The Illustrated Wavelet Transform Handbook: Introductory Theory and Applications in Science, Engineering, Medicine and Finance* (Physicist). Boca Raton, FL, USA: CRC Press, 2017.
[42] M. Ratsch, G. Teschke, S. Romdhani, and T. Vetter, "Wavelet frame accelerated reduced support vector machines," *IEEE Trans. Image Process.*, vol. 17, no. 12, pp. 2456–2464, Dec. 2008.
[43] J. Jiang, J. Ma, C. Chen, Z. Wang, Z. Cai, and L. Wang, "SuperPCA: A superpixelwise PCA approach for unsupervised feature extraction of hyperspectral imagery," *IEEE Trans. Geosci. Remote Sens.*, vol. 56, no. 8, pp. 4581–4593, Aug. 2018.
[44] L. Yang, Z. Zeng, and X. Shi, "A memristor-based neural network circuit with synchronous weight adjustment," *Neurocomputing*, vol. 363, pp. 114–124, Oct. 2019.
[45] X. Feng, Y. Jiang, X. Yang, M. Du, and X. Li, "Computer vision algorithms and hardware implementations: A survey," *Integration*, vol. 69, pp. 309–320, Nov. 2019.

DAMIRA MUSSINA (Associate Member, IEEE) received the M.Sc. degree in energy from Heriot-Watt University, Edinburgh, U.K., in 2013. She is currently pursuing the Ph.D. degree with the Department of Electrical and Digital Sciences, Nazarbayev University. From 2015 to 2018, she worked as a teaching assistant from 2017 to 2019. She was a Research Assistant with the School of Engineering and Computer Sciences, Nazarbayev University. Her research interests include machine learning, deep learning, image processing, and airborne imaging. Her current interests include the development of a remote-sensing inspection technique for high-voltage power lines using machine learning and deep learning methods. In 2012, she received the Scholarship of the Presidential Program for her M.Sc. Study in the U.K.

AIDANA IRMANOVA (Associate Member, IEEE) received the B.Sc. and M.Sc. degrees in information systems from PSU, Pavlodar, Kazakhstan, in 2014 and 2016, respectively. She is currently pursuing the Ph.D. degree with the Department of Electrical and Digital Sciences, Nazarbayev University. From 2016 to 2020, she worked as a Research Assistant with the School of Engineering and Computer Sciences, Nazarbayev University. Her research interests include analog memory design, memristive neuromorphic mixed signal circuits, and neural network architectures.

PRASHANT K. JAMWAL (Senior Member, IEEE) received the Ph.D. degree from the University of Auckland, New Zealand. Earlier he graduated from IIT, India, securing first position in all the disciplines. He is currently working with the School of Engineering and Design Sciences, Nazarbayev University, Nur-Sultan, Kazakhstan. He is actively pursuing research in artificial intelligence, multi-objective evolutionary optimization, bio-mechatronics, and robotics. He has developed medical robots for rehabilitation and surgical applications besides the development of improved algorithms for cancer data analytics. He is a member of many IEEE societies including the robotics and automation society. Besides editorial and publishing work, he has won many awards such as best paper awards, best digital solution award for his medical robots, Asian Universities Alliance (AUA) Scholars Award, and so on. He is a member of many IEEE societies including the robotics and automation society. Recently, United Nations acknowledged one of his robotics projects as one of the top twenty innovative projects in the world. He has led many government funded research projects including a prestigious World Bank grant. He received the Postdoctoral Fellowship from the University of Auckland.

MEHDI BAGHERI (Senior Member, IEEE) received the M.Sc. degree in power engineering from the Sharif University of Technology, Tehran, Iran, in 2007, and the Ph.D. degree in electrical power engineering and energy systems from the University of New South Wales (UNSW), Sydney, Australia. He has been with the Electrical Engineering Department, National University of Singapore (NUS), from 2015 to 2016. He closely worked with the Rolls-Royce Pte., Ltd., Singapore, on Condition Monitoring and Predictive Maintenance of Marine Transformers and Filters. He is currently an Associate Professor with the School of Engineering and Digital Sciences, Nazarbayev University, Nur-Sultan, Kazakhstan. He has served as the Head of the Test and Diagnostic Department, ITRI, from 2008 to 2010, on a project titled Operation, Life Assessment and Maintenance of Transformers of Iran's Transmission Substations, 400 kV and 230 kV, a collaborative project between ITRI and Iran Grid Management Company (IGMC). His research interests include high-voltage engineering, condition monitoring and assessment, intelligent methods for energy systems, IoE, electric vehicles and dynamic wireless charging, diagnosis in power systems for off- and onshore applications, electrical rotating machines, transient in power systems, electrical insulation, power quality, smart grid and city, demand response, and smart energy systems. He is currently an Associate Editor with IEEE Access Journal, a member of the IEEE Dielectrics and Electrical Insulation (DEIS), and the IEEE Power and Energy (PES) Societies, and the National Research Council Member of Kazakhstan. He is the Head of the Smart Energy Solution Laboratory.